NEAR-BLOWOFF DYNAMICS OF BLUFF-BODY-STABILIZED PREMIXED HYDROGEN/AIR FLAMES IN A NARROW CHANNEL

Bok Jik Lee*, Chun Sang Yoo, Hong G. Im***
bokjik.lee@kaust.edu.sa
*Clean Combustion Research Center, King Abdullah University of Science and Technology, Thuwal 23955-6900, Saudi Arabia
**School of Mechanical and Nuclear Engineering, Ulsan National Institute of Science and Technology, Ulsan 689-798, Korea

Abstract
The flame stability is known to be significantly enhanced when the flame is attached to a bluff-body. The main interest of this study is on the stability of the flame in a meso-scale channel, considering applications such as combustion-based micro power generators. We investigate the dynamics of lean premixed hydrogen/air flames stabilized behind a square box in a two-dimensional meso-scale channel with high-fidelity numerical simulations. Characteristics of both non-reacting flows and reacting flows over the bluff-body are studied for a range of the mean inflow velocity. The flame stability in reacting flows is investigated by ramping up the mean inflow velocity step by step. As the inlet velocity is increased, the initially stable steady flames undergo a transition to an unsteady mode of regular asymmetric fluctuation. When the inlet velocity is further increased, the flame is eventually blown off. Between the regular fluctuation mode and blowoff limit, there exists a narrow range of the inlet velocity where the flames exhibit periodic local extinction and recovery. Approaching further to blowoff limit, the local extinction and recovery becomes highly transient and a failure of recovery leads blowoff and extinction of the flame kernel.

Introduction
Towards the development of combustion-based micro-device for power generation [1, 2], there have been efforts to understand the combustion characteristics of premixed flame in meso-scale combustors, in particular for the flame stability.

Recent studies have reported that the blowoff limit of hydrogen/air premixed flames in a micro-combustor can be significantly extended by a bluff-body flame stabilizer [3, 4, 5, 6]. While a bluff-body has a desirable effect on flame stabilization by the help of a recirculation zone formed behind it, it also has some adverse effects on the stability of the flame anchored to it by shedding vortices to the flow [7, 8, 9], which may cause fluctuation of flames.

Experimental observations and diagnostics of hydrogen/air flames in meso-scale combustors are quite limited due to the small scales in space and time, and the weakness of luminosity. Although flame pictures taken from experiments [3], for instance, indicate the presence of flame behind the bluff-body in a planar micro-combustor, the flame structure and dynamics are largely unknown from them.

In the present study, high-fidelity numerical simulations are carried out to investigate the onset of instability of hydrogen/air premixed flames in a meso-scale channel with a square bluff-body. Through two-dimensional numerical simulations for a range of inflow velocities near the blowoff limit, flame dynamics and associated combustion characteristics are examined and discussed.

Computational setup

A two-dimensional computational domain (Fig. 1) is set for a channel of $D = 1$ mm height and $10D$ length. A bluff-body flame stabilizer is modelled by a square cylinder of size $0.5D$ by $0.5D$, whose center is located at $2.25D$ (i.e., the leading edge is at $2D$) downstream of the inflow boundary. To fully resolve reaction layers, a Cartesian grid system using a uniform grid spacing of $\Delta x = 5$ μm is chosen.

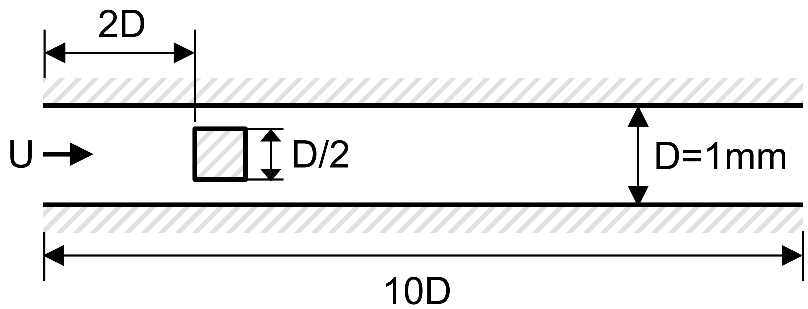

Figure 1: A two-dimensional computational domain for a narrow channel with a square-cylinder flame stabilizer

Numerical methods

Fully compressible, multi-species reactive Navier-Stokes equations are solved with a high-fidelity finite difference method using 8th order central difference and 4th order explicit Runge-Kutta time integration. For a lean hydrogen/air mixture of equivalence ratio of 0.5, a detailed reaction mechanism [10] with 9 species and 19 reactions is used. Chemical kinetics, thermodynamics, and transport properties are calculated using Chemkin libraries [11, 12]. A mixture-averaged model for species diffusion coefficients is applied. For parallel computing, the domain decomposition with MPI communications is employed, using 80 Intel Xeon CPU cores per each case.

For the inclusion of bluff-body geometry in the computational domain, an embedded boundary method is implemented. In this study, the square cylinder geometry is modelled as a union of logical MPI blocks, which is flagged to be excluded from the computational domain. The boundaries along the geometry are regarded as non-communicating physical boundaries, just like the computational domain boundaries. Any boundary conditions and one-sided derivatives used for domain boundaries are then equally applicable to the embedded boundaries.

No-slip, adiabatic conditions are applied to the channel walls and bluff-body surfaces. The heat loss to the isolated small-scale bluff-body is negligible and as such, the adiabatic assumption on the bluff-body is reasonable. Simulations using constant temperature condition and adiabatic condition for channel walls showed no difference in flame dynamics attached to the bluff-body. Non-reflecting characteristic boundary conditions are applied for both inflow and outflow boundaries [13, 14]. A fully developed channel flow velocity profile with mean inflow velocity U is imposed at the inflow boundary, with temperature $T = 298$ K and pressure $p = 1$ atm. Cases with a mean inflow velocity U ranging from 15 m/s to 25 m/s are investigated.

Non-reacting flow simulations

Prior to reacting flow simulations, non-reacting flow simulations are conducted to explore the characteristics of flows around the bluff-body in a meso-scale channel, for the inflow velocity range of interest.

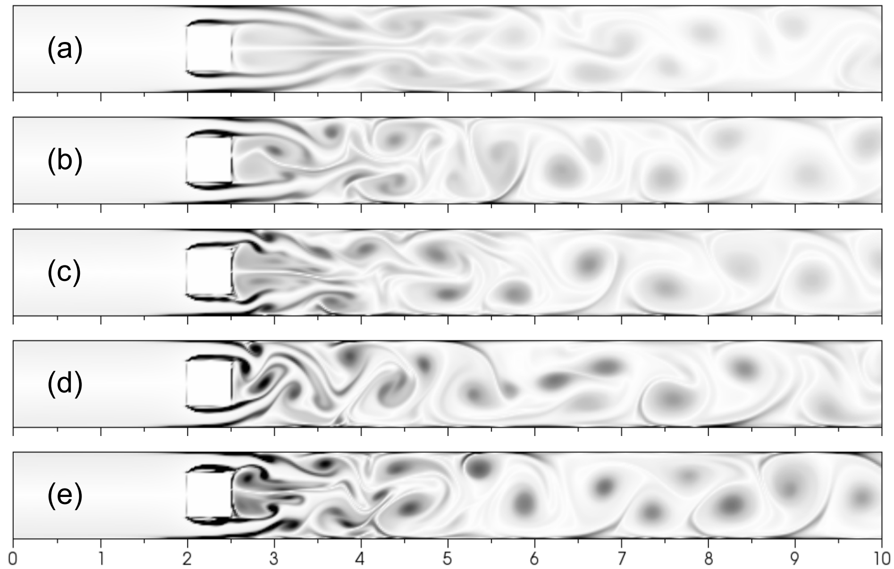

Figure 2: Contours of magnitude of vorticity at (a) U = 15 m/s, (b) 18 m/s, (c) 20 m/s, (d) 22 m/s, and (e) 25 m/s at t = 10 ms

Figure 2 shows the magnitude of vorticity for the inflow velocity U from 15 m/s to 25 m/s. The maximum magnitude for the contour plots is set to be 10^6/s. Strong shear layers are developed along the channel walls and the sides of the bluff-body, producing pairs of vortices into both sides of the downstream flow. The separation zones formed on both sides of the bluff-body are repeatedly opened and closed at the trailing edge due to the interaction of the flow with the recirculation zone at the base of the bluff-body. The flows behind the bluff-body are then unsteady and asymmetric, and the vortex-shedding becomes stronger and more asymmetric as the mean inflow velocity is increased.

The frequency f of asymmetric shedding of the vortices is approximately 20 kHz for the non-reacting cases, and the corresponding Strouhal number, defined by $2fD/U$, is about 0.5 . The flow residence time in the channel, i.e., the flow-through time, is 0.5 ms at U = 20 m/s for instance. Reynolds number based on the height of the bluff-body is around 500.

Steady stable flame

At U = 15 m/s, flame is stabilized at both sides near the trailing edge of the bluff-body, keeping symmetric shape without any fluctuations. The shedding of vortices observed in the non-reacting flow case in Fig. 2 (a) at the same inflow velocity is suppressed in the reacting case, as shown in Fig. 3. The maximum value of heat release rate for the contour plots in following sections are set to be 10^{10} J/m-s.

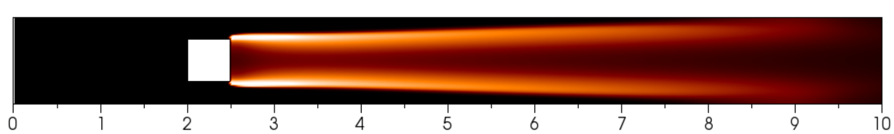

Figure 3: Contours of heat release rate for U = 15 m/s

This kind of steady stable mode of flame is maintained up to the mean inflow velocity being less than 19 m/s.

Transition to unstable flame

At the mean inflow velocity $U = 19$ m/s, a transition from steady flame to unsteady asymmetric flame starts to occur over time. As shown in Fig. 4, the flame which remains steady and symmetric until $t = 4.0$ ms undergoes a transition to an unstable mode in which the flame attached to the bluff-body fluctuates, showing a overall shape similar to sawtooth waves.

Figure 5 shows this transition in terms of total heat release rate across the domain over time. Once triggered, the instability builds up rapidly within a flow-through time. When the flame is in unstable mode, regular fluctuations coupled with asymmetric vortex shedding are observed. The frequency of fluctuations is about 60 kHz, which corresponds to a Strouhal number of 1.5.

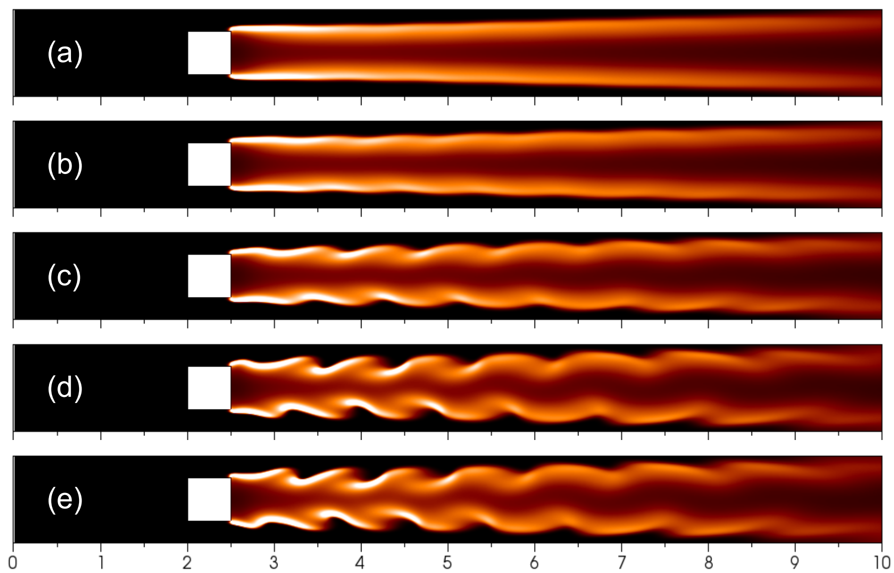

Figure 4: Contours of heat release rate for $U = 19$ m/s at (a) $t = 4.0$ ms, (b) 4.2 ms, (c) 4.4 ms, (d) 4.6 ms, and (e) 4.8 ms

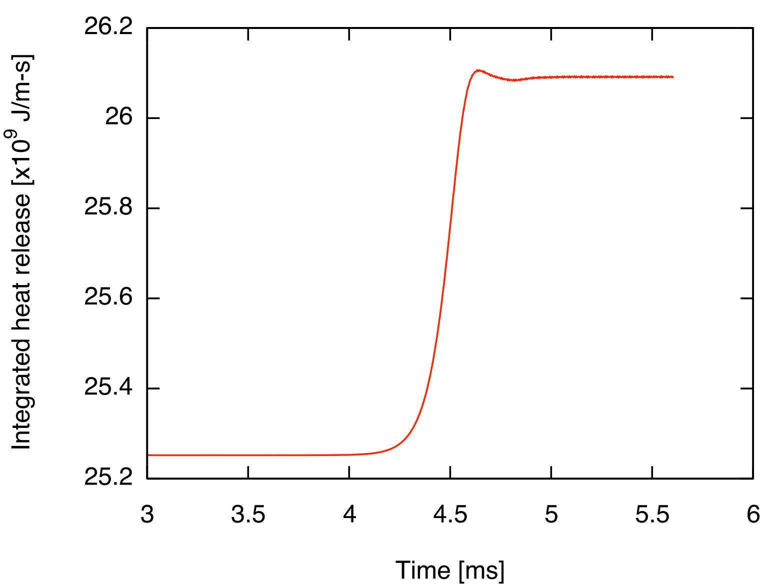

Figure 5: Temporal evolution of heat release rate integrated over the domain

When the mean inflow velocity is increased from 19 m/s to 20 m/s, the regular fluctuations of the flame are continued (Fig 6). Although it is not noticeable, the overall shape of the flame becomes narrower in the downstream of the bluff-body and the number of curved flamelets of peak heat release behind the trailing edge is decreased, comparing to those at $U = 19$ m/s.

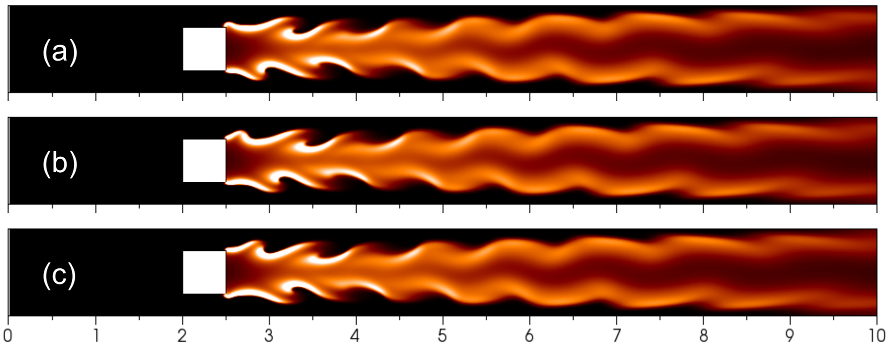

Figure 6: Contours of heat release rate for $U = 20$ m/s at (a) $t = 3.0$ ms, (b) 4.0 ms, and (c) 5.0 ms

The increase of the mean inflow velocity for all the cases greater than 19 m/s is done by ramping it up smoothly to a target velocity for a flow-through time by restarting the simulation from the solution at the mean inflow velocity of $U = 19$ m/s, and at time $t =$ 5 ms which is the moment when the flame is regularly fluctuating after the transition to the unstable mode. Upon restarting, the simulation time is reset to zero ($t = 0$).

Periodic local extinction and recovery

The flame becomes sensitive to a small change of the mean inflow velocity when the mean inflow velocity is further increased to U greater than 20 m/s. At $U = 20.5$ m/s, another mode of instability grows leading to a limit cycle of local extinction and recovery of the flame. Figure 7 shows time history of the heat release rate measured at a point located 2 D distance along the center line behind the base of the bluff-body. A zoomed-in plot at the limit cycle is shown for clarity. The local extinction and recovery is repeated periodically in this limit cycle at a frequency of 15 kHz approximately.

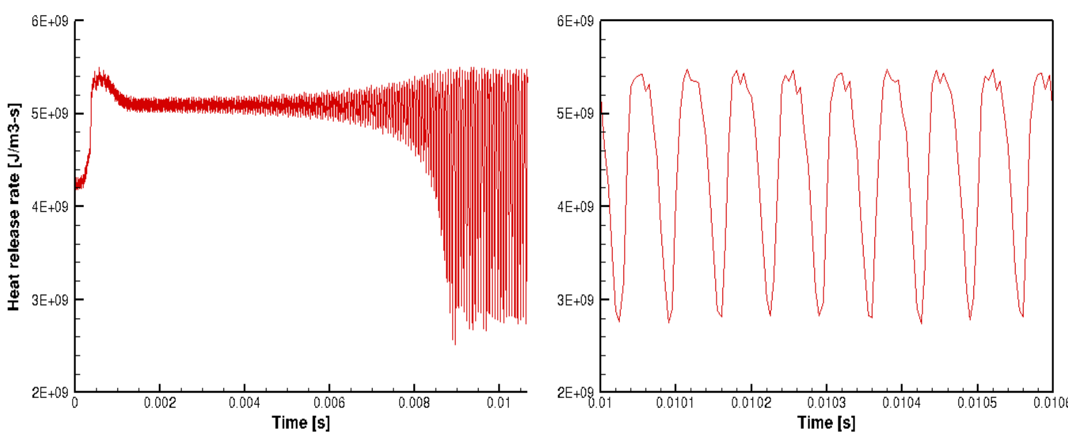

Figure 7: Temporal evolution of local heat release rate at $x = 4.25D$ for $U = 20.5$ m/s

Flame dynamics undergoing the repetition of local extinction and recovery at the limit cycle is shown in Fig. 8. Local extinction occurs at about $2D$ downstream of the bluff-body base, near the downstream end of the recirculation zone. Despite of the strong shear strain of the flow behind the trailing edges of the bluff-body, flamelets are able to anchor to the bluff-body because of the heat supply maintained by the recirculation in the base region, keeping the local conditions away from the extinction limit. Therefore, the local flame extinction occurs at a point where the heat supply from the recirculation zone is not sufficient due to the reattachment of the flow behind the bluff-body.

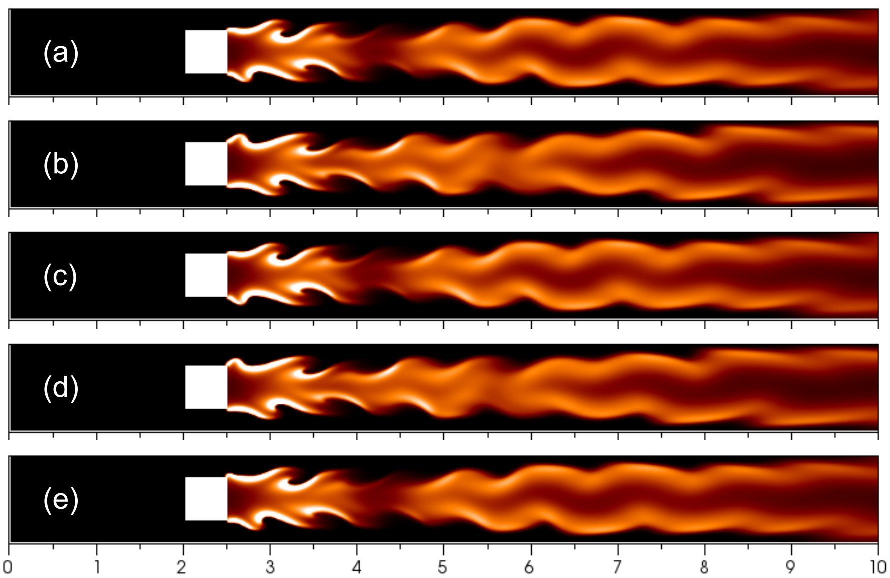

Figure 8: Contours of heat release rate for U = 20.5 m/s at (a) t = 10.09 ms, (b) 10.13 ms, (c) 10.16 ms, (d) 10.20 ms, and (e) 10.23 ms

Some other quantities are selected to illustrate the states at the local extinction phase in the cycle in Fig. 9. It shows the production of OH radical is decreased as soon as the recirculation zone is closed.

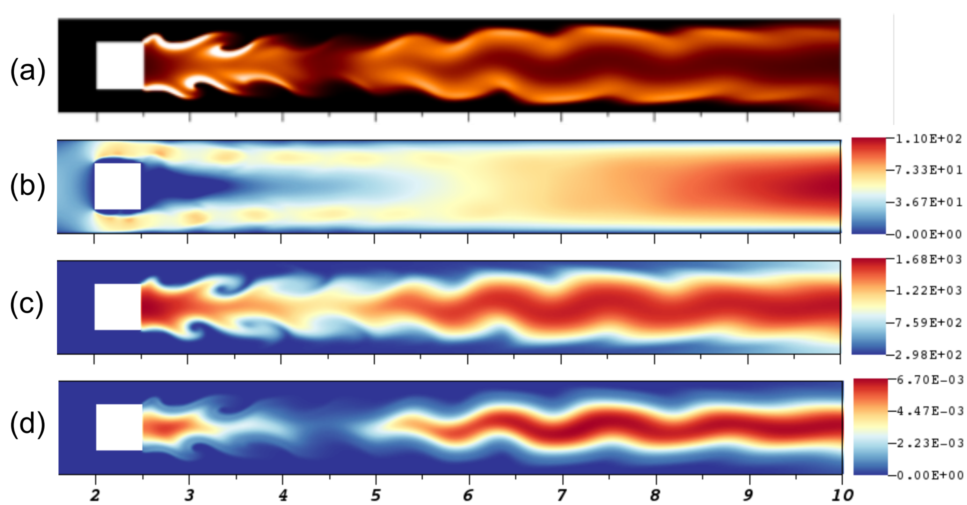

Figure 9: Local extinction phase for U = 20.5 m/s; Contours of (a) heat release rate, (b) axial velocity, (c) temperature, and (d) Y_{OH}

Blowoff

At slightly higher velocity of U = 20.6 m/s, the flame eventually fails to be recovered over time, leading to the blowoff of bulk of the flame and to the complete extinction. In this section, highly unstable dynamics of the flame at the very near condition of blowoff is depicted with key sequences of event over time.

At earlier stage at $U = 20.6$ m/s, periodic local extinction and recovery mode is found, as shown in Fig. 10.

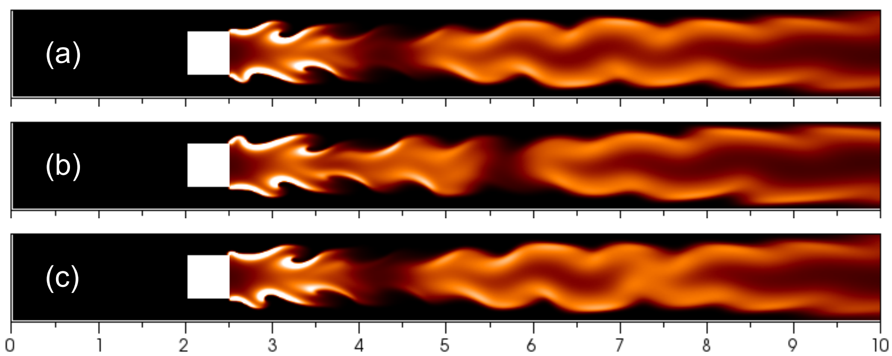

Figure 10: Contours of heat release rate for $U = 20.6$ m/s at (a) $t = 1.82$ ms, (b) 1.86 ms, and (c) 1.89 ms

At later stage, the flame exhibits local extinction and recovery irregularly, then the detached bulk flame generated by the local extinction is blown off at a certain point of time as illustrated in Fig. 11.

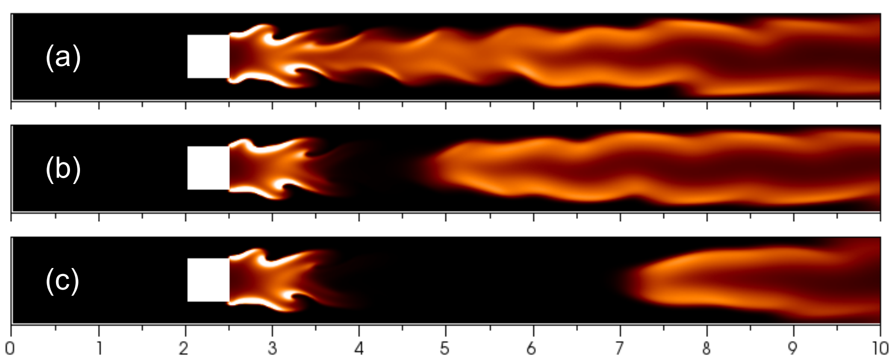

Figure 11: Contours of heat release rate for $U = 20.6$ m/s at (a) $t = 2.84$ ms, (b) 2.9 ms, and (c) 3.0 ms

After the bulf flame is blown off, the remaining flame kernel sometimes grows back to full flame as shown in Fig. 12.

At around $t = 3.45$ ms shown in Fig. 13, the local extinction and detachment of the bulk flame is not recovered, and the remaining flame kernel does not grow back to full flame. This leads to a complete extinction of the flame.

While both Fig. 11 (c) and Fig. 13(b) show the blowoff of detached bulk flames, there is difference between them in that the shrinking of the flame kernel attached to the bluff-body is in progress for the case of Fig. 13(b). Being at a critical balance condition between the competition of flow residence time and the time required for the ignition at this local area, The ignition of locally unreacted mixture at the local extinction area depends on the competition of flow residence time and the time required for the ignition at this local area. Being at such a critical balance condition at near-blowoff regime, the local extinction is at the saddle point between recovery and irrevocable blowoff.

The overall time history of the heat release rate measured at a point located $2D$ distance along the center line behind the base of the bluff-body at $U = 20.6$ m/s is shown in Fig. 14. Comparing to Fig. 7, the development of the instability involving local

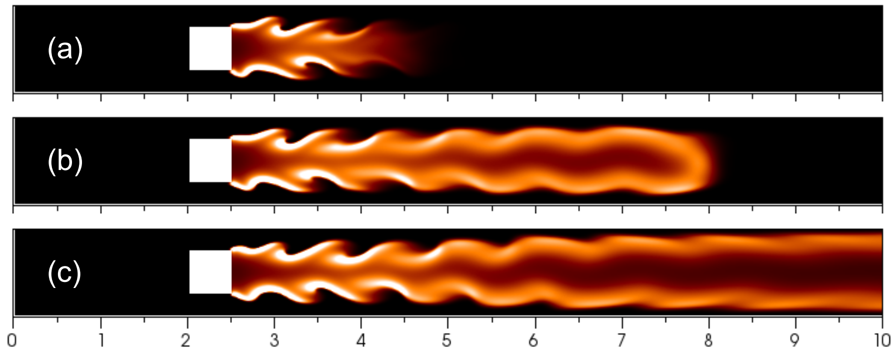

Figure 12: Contours of heat release rate for $U = 20.6$ m/s at (a) $t = 3.2$ ms, (b) 3.27 ms, and (c) 3.32 ms

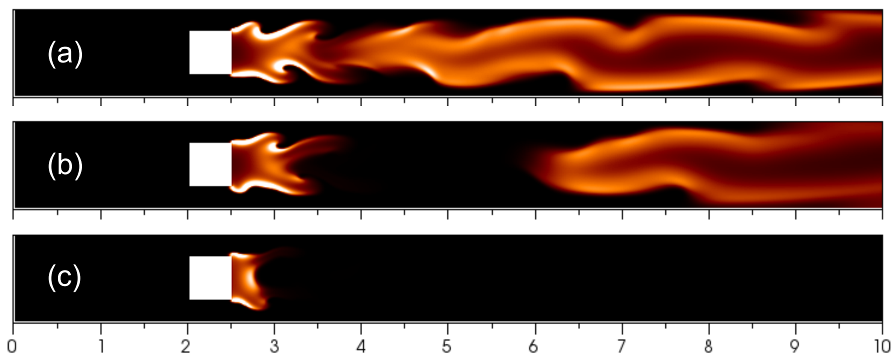

Figure 13: Contours of heat release rate for $U = 20.6$ m/s at (a) $t = 3.4$ ms, (b) 3.45 ms, and (c) 3.75 ms

extinction and recovery becomes highly unstable and intermittent after $t = 1.8$ ms. Local heat release rate becomes zero at around $t = 3$ ms, then is soon recovered to its normal value due to the growth of the flame kernel attached to the bluff-body. However, the disappearance of the heat release rate after $t = 3.5$ ms involves shrinking flame kernel leading to complete extinction of the flame.

Discussion

The onset of local extinction generating holes in the flame at around $U = 20.5$ m/s in the present study agrees qualitatively with experimental observations at the near-blowoff limit of lean or stoicheometric mixtures for lager scale flames reported.

In the experiments of Yamaguchi et al. [15], using stoichiometric propane/air mixture at $U = 10$ m/s in a channel of 60 mm width, the blowoff of the rod-stabilized flame was observed to be triggered by a local extinction of the stretched eddy-flames at the end of recirculation zone.

Nair and Lieuwen [16] observed the flame dynamics around a cylindrical rod of diameter 9.5 mm at $U = 1.2$ m/s for a range of lean natural gas and air mixtures at near blowoff conditions under nearly unconfined condition. A two-stage scenario was suggested: the first stage manifested by the presence of localized holes at locations where the instantaneous stretch rate exceeds the extinction stretch rate, and the second stage that occurs at further decreased equivalence ratio and involves large-scale alterations of the wake dynamics.

Chaudhuri et al. [17] studied bluff-body stabilized flame dynamics near the lean blowoff of propane/air mixtures using time-resolved chemiluminescence imaging and si-

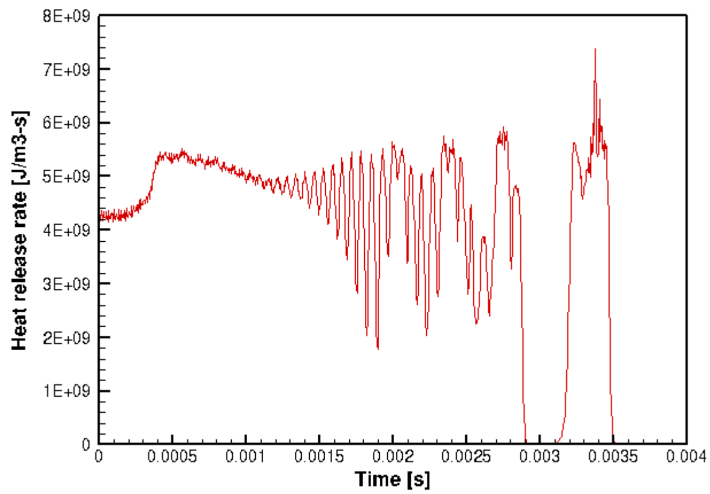

Figure 14: Temporal evolution of local heat release rate at $x = 4.25D$ for $U = 20.6$ m/s

multaneous PIV and OH PLIF. A hypothesis was constructed for the lean blowoff mechanism that includes partial flame extinction followed by either successful reignition or failure of reignition leading to blowoff.

The dynamics of the hydrogen/air bluff-body stabilized flame in a meso-scale channel at near-blowoff illustrated in the present study is largely consistent with the observations and hypothesis from the previous experiments mentioned above. In the present study, however, we have identified two different scenarios for the recovery of the flame after having the hole of local extinction: (1) reunion of flame kernels attached to the bluff-body and the detached bulk flame when the extinction hole is small enough, and (2) regrowth of the flame from the flame kernels when the extinction hole is so large that the detached bulk flame is blown off. If the second scenario fails to occur, then the flame kernel is eventually shrunken leading to complete extinction.

Conclusion

In the present study, two-dimensional direct numerical simulations for bluff-body stabilized flames of a lean mixture of hydrogen/air at near-blowoff conditions in a meso-scale channel have illustrated a variety of transient characteristics in flame dynamics.

From a series of numerical experiments by ramping up the mean inflow velocity, it has been found that when the inflow velocity approaches to blowoff limit, there exist distinct modes of the flame dynamics before a stable flame is blown off along the increase of the inflow velocity: (1) steady symmetic flame, (2) regular asymmetic fluctuation, (3) periodic local extinction and recovery by reunion, (4) highly transient local extinction and recovery by regrowth, and (5) failure of recovery leading to blowoff.

Further analysis needs to be done on the competition between flow time scale and chemical time scale to find the conditions determining various modes of flame dynamics described above, and the limit conditions of blowoff.

References

[1] Maruta, K., "Micro and mesoscale combustion", *Proceedings of the Combustion Institute* 33:125–150 (2011).

[2] Kaisare, N.S., Vlachos, D.G., "A review on microcombustion: Fundamentals, devices and applications", *Progress in Energy and Combustion Science* 38:321–359 (2012).

[3] Wan, J., Fan, A., Maruta, K., Yao, H., Liu, W., "Experimental and numerical investigation on combustion characteristics of premixed hydrogen/air flame in a micro-combustor with a bluff body", *International Journal of Hydrogen Energy* 37:19190–19197 (2012).

[4] Fan, A., Wan, J., Maruta, K., Yao, H., Liu, W., "Interactions between heat transfer, flow field and flame stabilization in a micro-combustor with a bluff body", *International Journal of Heat and Mass Transfer* 66:72–79 (2013).

[5] Fan, A., Wan, J., Liu, Y., Pi, B., Yao, H., Maruta, K., Liu, W., "The effect of the blockage ratio on the blow-off limit of a hydrogen/air flame in a planar micro-combustor with a bluff body", *International Journal of Hydrogen Energy* 38:11438–11445 (2013).

[6] Bagheri, G., Hosseini, S.E., Wahid, M.A., "Effects of bluff body shape on the flame stability in premixed micro-combustion of hydrogenair mixture", *Applied Thermal Engineering* 67:266–272 (2014).

[7] Suzuki, H., Inoue, Y., Nishimura, T., Fukutani, K., Suzuki, K., "Unsteady flow in a channel obstructed by a square rod (crisscross motion of vortex)", *International Journal of Heat and Fluid Flow* 14:2–9 (1993).

[8] Suzuki, K., Suzuki, H., "Instantaneous structure and statistical feature of unsteady flow in a channel obstructed by a square rod", *International Journal of Heat and Fluid Flow* 15:426–437 (1994).

[9] Hertzberg, J., Shepherd, I., Talbot, L., "Vortex shedding behind rod stabilized flames", *Combustion and Flame* 86:1–11 (1991).

[10] Li, J., Zhao, Z., Kazakov, A., Dryer, F.L., "An updated comprehensive kinetic model of hydrogen combustion", *International Journal of Chemical Kinetics* 36:566–575 (2004).

[11] Kee, R.J., Rupley, F.M., Miller, J.A., "CHEMKIN-II: A FORTRAN Chemical Kinetics Package for the Analysis of Gas-Phase Chemical Kinetics", Tech. Rep. SAND89-8009, Sandia National Laboratories (1989).

[12] Kee, R.J., Dixon-Lewis, G., Warnatz, J., E., C.M., Miller, J.A., "A FORTRAN Computer Code Package for the Evaluation of Gas-Phase, Multicomponent Transport Properties", Tech. Rep. SAND86-8246, Sandia National Laboratories (1986).

[13] Yoo, C.S., Wang, Y., Trouvé, A., Im, H.G., "Characteristic boundary conditions for direct simulations of turbulent counterflow flames", *Combustion Theory and Modelling* 9:617–646 (2005).

[14] Yoo, C.S., Im, H.G., "Characteristic boundary conditions for simulations of compressible reacting flows with multi-dimensional, viscous and reaction effects", *Combustion Theory and Modelling* 11:259–286 (2007).

[15] Yamaguchi, S., Ohiwa, N., Hasegawa, T., "Structure and blow-off mechanism of rod-stabilized premixed flame", *Combustion and Flame* 62:31–41 (1985).

[16] Nair, S., Lieuwen, T.C., "Near-Blowoff Dynamics of a Bluff-Body Stabilized Flame", *Journal of Propulsion and Power* 23:421–427 (2007).

[17] Chaudhuri, S., Kostka, S., Renfro, M.W., Cetegen, B.M., "Blowoff dynamics of bluff body stabilized turbulent premixed flames", *Combustion and Flame* 157:790–802 (2010).